BRAIN
ORIGINAL ARTICLE

Disentangling the effects of Alzheimer's and small vessel disease on white matter fibre tracts

Anna Dewenter,[1] Mina A. Jacob,[2] Mengfei Cai,[2] Benno Gesierich,[1,3] Paul Hager,[1,4] Anna Kopczak,[1] Davina Biel,[1] Michael Ewers,[1,5] Anil M. Tuladhar,[2] Frank-Erik de Leeuw,[2] Martin Dichgans,[1,5,6] Nicolai Franzmeier,[1,†] and Marco Duering[1,3,†] for the SVDs@target Consortium and Alzheimer's Disease Neuroimaging Initiative (ADNI)

[†]These authors contributed equally to this work.

See Koops and Jacobs (https://doi.org/10.1093/brain/awac493) for a scientific commentary on this article.

Alzheimer's disease and cerebral small vessel disease are the two leading causes of cognitive decline and dementia and coexist in most memory clinic patients. White matter damage as assessed by diffusion MRI is a key feature in both Alzheimer's and cerebral small vessel disease. However, disease-specific biomarkers of white matter alterations are missing. Recent advances in diffusion MRI operating on the fixel level (fibre population within a voxel) promise to advance our understanding of disease-related white matter alterations. Fixel-based analysis allows derivation of measures of both white matter microstructure, measured by fibre density, and macrostructure, measured by fibre-bundle cross-section. Here, we evaluated the capacity of these state-of-the-art fixel metrics to disentangle the effects of cerebral small vessel disease and Alzheimer's disease on white matter integrity.

We included three independent samples (total $n = 387$) covering genetically defined cerebral small vessel disease and age-matched controls, the full spectrum of biomarker-confirmed Alzheimer's disease including amyloid- and tau-PET negative controls and a validation sample with presumed mixed pathology. In this cross-sectional analysis, we performed group comparisons between patients and controls and assessed associations between fixel metrics within main white matter tracts and imaging hallmarks of cerebral small vessel disease (white matter hyperintensity volume, lacune and cerebral microbleed count) and Alzheimer's disease (amyloid- and tau-PET), age and a measure of neurodegeneration (brain volume).

Our results showed that (i) fibre density was reduced in genetically defined cerebral small vessel disease and strongly associated with cerebral small vessel disease imaging hallmarks; (ii) fibre-bundle cross-section was mainly associated with brain volume; and (iii) both fibre density and fibre-bundle cross-section were reduced in the presence of amyloid, but not further exacerbated by abnormal tau deposition. Fixel metrics were only weakly associated with amyloid- and tau-PET. Taken together, our results in three independent samples suggest that fibre density captures the effect of cerebral small vessel disease, while fibre-bundle cross-section is largely determined by neurodegeneration. The ability of fixel-based imaging markers to capture distinct effects on white matter integrity can propel future applications in the context of precision medicine.

1 Institute for Stroke and Dementia Research (ISD), University Hospital, LMU Munich, Germany
2 Department of Neurology, Donders Institute for Brain, Cognition and Behaviour, Radboud University Medical Center, Nijmegen, The Netherlands

Received March 03, 2022. Revised May 30, 022. Accepted June 25, 2022. Advance access publication July 21, 2022

3 Medical Image Analysis Center (MIAC) and Department of Biomedical Engineering, University of Basel, Basel, Switzerland
4 Institute for AI and Informatics in Medicine, Klinikum rechts der Isar, Technical University of Munich, Munich, Germany
5 German Center for Neurodegenerative Disease (DZNE), Munich, Germany
6 Munich Cluster for Systems Neurology (SyNergy), Munich, Germany

Correspondence to: Marco Duering
Medical Image Analysis Center (MIAC AG)
Marktgasse 8
CH-4051 Basel
Switzerland
E-mail: marco.duering@miac.ch

Keywords: Alzheimer's disease; cerebral small vessel disease; fixel-based analysis; diffusion magnetic resonance imaging; CADASIL

Introduction

Alzheimer's disease and cerebral small vessel disease (SVD) are the two most frequent causes of dementia.[1,2] Alzheimer's disease is a proteinopathy characterized by the cortical accumulation of amyloid-beta (Aβ) plaques and neurofibrillary tau tangles that lead to neurodegeneration, which can be assessed using PET and MRI.[3] In contrast, SVD is associated with pathological alterations of small penetrating vessels that manifest on MRI mainly as white matter hyperintensities, lacunes and cerebral microbleeds.[4,5] While Alzheimer's disease and SVD are distinct diseases with different aetiologies and pathomechanisms, the majority of patients who seek clinical care in memory clinics present with both Alzheimer's disease- and SVD-related brain alterations to varying degrees. Histopathology studies have shown that up to 80% of patients with prodromal Alzheimer's disease show cerebrovascular alterations upon autopsy.[6] This suggests substantial overlap between both disease entities in clinical populations, probably due to shared risk factors.[6–8] Hence, there is a great need for biomarkers that capture both Alzheimer's disease and SVD and describe the extent and contribution of each disease within the individual patient.

In recent years, diffusion MRI has evolved as the method of choice to quantify white matter alterations in SVD, with most studies relying on diffusion tensor imaging.[9,10] Diffusion alterations in the white matter are also frequently observed across the Alzheimer's disease continuum.[11,12] Global white matter diffusion metrics seem largely determined by SVD-related white matter damage, masking any white matter damage that might occur due to Alzheimer's disease pathology.[13] Studies using regions-of-interest or tract-based analysis suggest different spatial patterns of diffusion MRI alterations in Alzheimer's disease and SVD, which warrants study on regional effects on white matter fibre tracts.[14,15] However, specific biomarkers for Alzheimer's disease- and SVD-related white matter damage are still missing.

A potential reason why previous diffusion models failed to disentangle white matter alterations due to different pathologies is their inability to account for the complex anatomy of brain white matter.[16] Histology studies show that the brain's white matter architecture is highly complex, with up to 98% of the white matter consisting of multiple fibres with crossing fibre orientations.[17,18] State-of-the-art constrained spherical deconvolution algorithms yield promise because they allow derivation of diffusion measures specific to underlying fibre populations, i.e. on the 'fixel' (fibre population within a voxel) instead of the voxel level (Fig. 1).[19] Using this framework, one can simultaneously derive tract-specific measures of fibre density and fibre-bundle cross-section. Fibre density is a fixel-specific feature of white matter 'microstructure', approximately proportional to the total intra-axonal volume.[20] Fibre-bundle cross-section is a fixel-specific 'macroscopic' feature, presumably reflecting the accumulated axon loss.[19,21]

The first fixel-based study in clinical Alzheimer's disease and mild cognitive impairment reported reductions in both fibre density and fibre-bundle cross-section of main fibre tracts compared with cognitively healthy controls.[22] However, it remains elusive, (i) whether amyloid and tau pathology is associated with fibre density or fibre-bundle cross-section; and (ii) whether this association is altered in sporadic Alzheimer's disease with comorbid SVD. The ability of fibre density and fibre-bundle cross-section to describe and disentangle the effects of SVD and Alzheimer's disease pathology on white matter integrity within the same patient has not been explored so far.

To address the need for disease-specific markers, the first aim of this study was to assess the effects of both SVD and biomarker-confirmed Alzheimer's disease on both fibre density and fibre-bundle cross-section of major white matter fibre tracts compared with age-matched controls. Our second aim was to explore the relationship between well-established SVD MRI and Alzheimer's disease PET imaging hallmarks with tract-specific measures of fibre density and fibre-bundle cross-section. We addressed these aims using three independent samples (total $n = 387$) covering genetically defined SVD [cerebral autosomal dominant arteriopathy with subcortical infarcts and leukoencephalopathy (CADASIL)] and age-matched controls, sporadic Alzheimer's disease with full amyloid- and tau-PET-based biomarker characterization including controls without amyloid and tau pathology as well as a validation sample with mixed pathology. We combined conventional MRI markers and PET data with state-of-the-art fixel-based analyses of advanced diffusion MRI data. Our main goal was to disentangle white matter damage due to Alzheimer's disease and SVD using fixel-based metrics, opening the road for disease-specific white matter characterization towards precision medicine.

Materials and methods

Participants

We included three independent samples with 3 T multi-shell diffusion MRI (Fig. 2). First, to study the effect of SVD in isolation, we

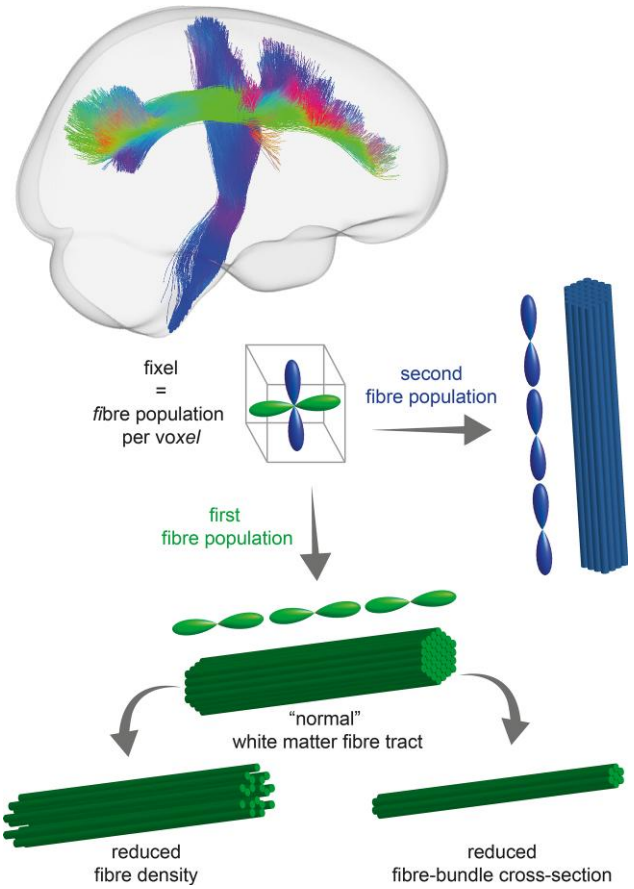

Figure 1 Illustration of fixel-based analysis of two exemplary crossing white matter fibre tracts (superior longitudinal fasciculus II in green, cortico-spinal tract in blue). A fixel corresponds to a specific fibre population per voxel. The depicted voxel harbours two fibre populations (colour-coded per tract). A reduction in fibre density (with preserved fibre-bundle cross-section) is depicted on the *left*, while a reduction in fibre-bundle cross-section (with preserved fibre density) is depicted on the *right*.

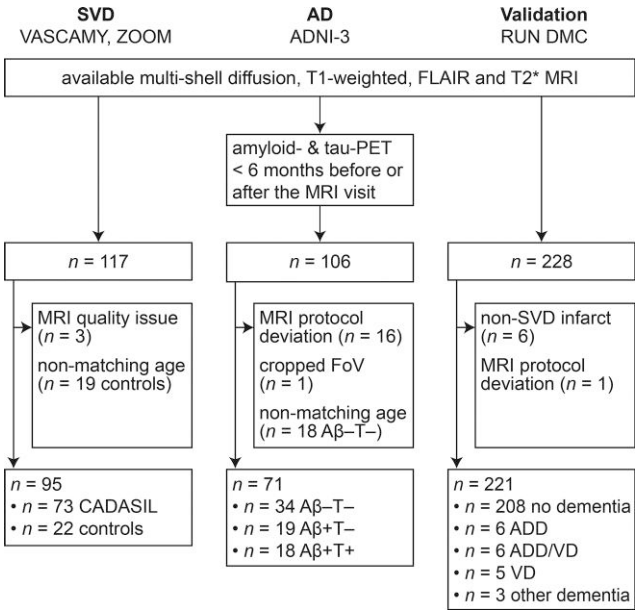

Figure 2 Participant selection flow chart. Samples included genetically defined cerebral SVD (CADASIL) and matched healthy controls (SVD sample), the full spectrum of Alzheimer's disease (AD) and a validation sample with presumed mixed pathology. ADD = Alzheimer's disease dementia; FoV = field of view; VD = vascular dementia.

included patients with genetically defined SVD and age-matched controls. Second, the effect of Alzheimer's disease was studied across the full spectrum of sporadic Alzheimer's disease pathology, ranging from age-matched controls without evidence of amyloid or tau pathology (Aβ–T–) to patients with amyloid pathology only (Aβ+T–) and patients with both amyloid and tau pathology (Aβ+T+). Lastly, we used a third study sample with presumed mixed pathology for independent validation.

Study protocols were in accordance with the Declaration of Helsinki and approved by local ethics committees. Written informed consent was obtained from all participants.

Small vessel disease sample

We included in total 95 participants with identical MRI acquisition on the same scanner from a single-centre cohort in Munich[10] ($n = 79$) and the ZOOM@SVDs study[23] ($n = 16$), of whom 73 were patients with genetically defined SVD (CADASIL) and 22 were healthy controls matched for age and sex on the group level. CADASIL patients were symptomatic, but in an early disease stage (i.e. functionally independent).

Alzheimer's disease sample

Participants from the Alzheimer's Disease Neuroimaging Initiative 3 (ADNI) database were selected based on availability of multi-shell diffusion MRI and structural MRI, as well as ^{18}F-florbetapir or ^{18}F-florbetaben amyloid-PET and ^{18}F-flortaucipir tau-PET within 6 months of the MRI visit ($n = 106$).[24] Seventeen participants were excluded due to relevant diffusion MRI protocol deviations ($n = 16$) or a cropped field of view ($n = 1$). Controls were matched for age and sex on the group level.

We used a biological definition of Alzheimer's disease following NIA-AA guidelines[3] and assigned participants as Aβ+ when surpassing a global pre-established Aβ positivity standardized uptake value ratio (SUVR) threshold of 1.11 for ^{18}F-florbetapir and 1.08 for ^{18}F-florbetaben amyloid-PET.[25] Tau positivity was assigned when surpassing a pre-established ^{18}F-flortaucipir SUVR threshold of 1.3 in any of the predefined Braak stage regions (Braak1, Braak3, Braak3/4, Braak4, Braak5, Braak5/6, Braak6).[26,27] Of note, the hippocampus (i.e. Braak2) was excluded from all analyses due to relevant off-target binding of the ^{18}F-flortaucipir tracer in the medial temporal lobe. As our main interest was in the neuropathological effects of amyloid and tau pathology on white matter tissue integrity, we used exclusively the biological definition of Alzheimer's disease and did not take clinical status into account. We included 71 participants, of whom 34 controls had no biomarker evidence for Alzheimer's disease pathology (Aβ–T–) and 37 Aβ+ individuals across the Alzheimer's disease spectrum (19 Aβ+T–, 18 Aβ+T+).

Validation sample

We selected participants from the third follow-up visit (approximately 14 years after baseline) of the RUN DMC study[28] (Radboud University Nijmegen Diffusion Tensor and Magnetic Resonance Cohort), based on the availability of multi-shell diffusion MRI ($n = 228$). We excluded six participants with infarcts of non-SVD aetiology and one participant due to an MRI protocol deviation, resulting in a final sample of 221 participants. While the cohort recruited

non-demented elderly with SVD, neurodegenerative pathologies were not excluded and during the long-term follow-up, some participants were in fact diagnosed with Alzheimer's disease dementia (Fig. 2).[29] Therefore, we refer to this sample as the validation sample with presumed mixed pathology. However, data on amyloid or tau, either PET or fluid biomarkers, were not available for these participants.

MRI acquisition and conventional MRI markers

Full sequence parameters are shown in Supplementary Table 1. Sequence parameters varied per study, but included 3D T_1-weighted, 3D fluid-attenuated inversion recovery (FLAIR) and 3D gradient echo (T_2*-weighted) sequences to assess conventional MRI markers [white matter hyperintensity volume (WMHV), lacune and cerebral microbleed count, brain volume (BrainV)] as well as a multi-shell diffusion MRI sequence. Conventional MRI markers were quantified according to consensus criteria.[4] All volumes were normalized to the intracranial volume (e.g. WMHV/intracranial volume).

Small vessel disease sample

MRI scans were performed on a single 3 T scanner (Magnetom Skyra with 64-channel head/neck coil; Siemens Healthineers). The diffusion MRI protocol comprised a multiband echo planar imaging multishell diffusion-weighted imaging sequence (repetition time 3800 ms, echo time 105 ms, diffusion-encoding directions: $30 \times b = 1000$ s/mm^2 and $60 \times b = 2000$ s/mm^2, 10 $b = 0$ images, multiband factor 3). One $b = 0$ image with inverted phase-encoding direction was acquired for correction of susceptibility-induced distortions during processing.[30,31] Details on the calculation of conventional MRI markers have been described previously.[10]

Alzheimer's disease sample

MRI scans were performed on different (in total 13) 3 T scanners (Magnetom Prisma or Magnetom Prisma Fit with 20-, 32- or 64-channel coils; Siemens Healthineers). The diffusion MRI protocol comprised a multiband echo planar imaging multi-shell diffusion-weighted sequence (repetition time 3400 ms, echo time 71 ms, diffusion-encoding directions $48 \times b = 1000$ s/mm^2 and $60 \times b = 2000$s/mm^2, 13 $b = 0$ images, multiband factor 3).

WMH were segmented using a deep-learning algorithm based on multidimensional gated recurrent units (https://github.com/zubata88/mdgru).[32] An expert rater blinded to biomarker status determined the number of lacunes on FLAIR and T_1-weighted images and the number of cerebral microbleeds on T_2*-weighted images. Brain and intracranial volumes were estimated from the T_1-weighted image with the cross-sectional Sequence Adaptive Multimodal SEGmentation (SAMSEG) Pipeline (FreeSurfer software suite, version 7.1).[33]

Validation sample

MRI scans were performed on a single 3 T scanner (Magnetom Prisma with 32-channel head coil; Siemens Healthineers). The diffusion MRI protocol comprised a multiband echo planar imaging multi-shell diffusion-weighted imaging sequence (repetition time 3220 ms, echo time 74 ms, diffusion-encoding directions $30 \times b = 1000$ s/mm^2 and $60 \times b = 3000$ s/mm^2, 10 $b = 0$ images, multiband factor 3). One $b = 0$ image with inverted phase-encoding direction was acquired for correction of susceptibility-induced distortions during processing. Details on the calculation of conventional MRI markers have been described previously.[34,35]

Diffusion MRI preprocessing

Preprocessing steps included visual quality control, Marchenko–Pastur principal component analysis-based denoising, Gibbs artefact removal and dynamic correction for susceptibility-induced distortions, eddy current-induced distortions, as well as head motion using tools from MRtrix3 (www.mrtrix.org/, version 3.0.0, dwidenoise,[36–39] mrdegibbs[39,40]) and the Functional Magnetic Resonance Imaging of the Brain Software Library (FSL, version 6.0.1, topup,[30,31] eddy[41] including state-of-the art replacement of outliers,[42] usage of the slice-to-volume motion model[43] and susceptibility-by-movement correction[44]). Due to unavailability of an unweighted diffusion image with reversed phase-encoding in the Alzheimer's disease sample, we used Synb0-DISCO to synthesize an unweighted diffusion image without susceptibility-induced distortion from the T_1-weighted image.[45,46] Other than this single step, preprocessing was kept identical across the three samples.

Tract-specific fixel-based analysis

We followed the fixel-based analysis pipeline recommended by the developers using multi-tissue constrained spherical deconvolution to compute fibre orientation distributions (FODs).[21,47] Fixel-based analyses were computed independently for each sample. Diffusion data was corrected for bias fields followed by a global diffusion-weighted imaging intensity normalization between subjects of each sample, yielding diffusion-weighted images with identical $b = 0$ white matter median intensity value. Response functions were estimated for each participant using the 'dhollander' algorithm,[48] based on which the mean response functions were computed. Remaining steps included upsampling to 1.25 mm voxel size, estimation of the FODs using the group response functions ('msmt_csd' algorithm) and intensity normalization. Next, study-specific FOD templates were calculated by randomly selecting representative participants, i.e. 15 controls and 15 CADASIL patients for the SVD sample, 15 Aβ–T– and 7 Aβ+T– and 8 Aβ+T+ for the Alzheimer's disease sample and 30 study participants from the validation sample. Subject-specific FOD images were registered to the FOD template, whereafter fixels were segmented and corresponding metrics of apparent fibre density, fibre-bundle cross-section and a combined measure of fibre density and cross-section were derived. As our main interest was to find disease-specific metrics for white matter damage, we focused on the primary metrics fibre density and fibre-bundle cross-section (but conducted supplementary analyses on the combined metric fibre density and bundle cross-section).

Next, we used TractSeg, a deep learning-based framework for automated white matter bundle segmentation, to segment the FOD template into 72 anatomically well-established white matter fibre tracts.[49] To reduce the number of comparisons, we averaged tract measures for left and right hemispheres. Also, to further reduce the number of regions of interest, we excluded the tracts located in the cerebellum—as it is to date unclear how SVD and Alzheimer's disease manifest in this brain area—as well as the fornix due to unavoidable CSF partial-volume effects. In addition, we excluded striatal projections from our analyses, due to a high anatomical overlap with thalamic projections. This resulted in 29 white matter fibre tracts (Fig. 3, from top left): arcuate fasciculus, uncinate fasciculus, inferior fronto-occipital fasciculus, middle longitudinal fasciculus, inferior longitudinal fasciculus, superior longitudinal fasciculus I to III, thalamo-prefrontal, thalamo-premotor, thalamo-precentral,

thalamo-postcentral, thalamo-parietal, thalamo-occipital, anterior thalamic radiation, superior thalamic radiation, optic radiation, fronto-pontine tract, cortico-spinal tract, parieto-occipital pontine, corpus callosum I to VII, anterior commissure, cingulum. We then assessed per study participant the fixel metrics per fibre tract by averaging the fibre density, fibre-bundle cross-section as well as fibre density and cross-section of all fixels belonging to the respective fibre tract.

To assess regional associations between regional tau pathology and tract-specific fixel metrics in the Alzheimer's disease sample, we determined regional tau-PET SUVRs in cortical projections of fibre tracts. To this end, we used masks from the beginning and ending of the fibre tracts, as obtained with TractSeg, intersected with a cortical grey matter mask. The regions of interest in FOD template space were brought to tau-PET images in MNI space by non-linear registration with Advanced Normalization Tools (ANTs)[50] to determine regional tau-PET SUVRs.

PET acquisition and processing

Amyloid-PET was recorded in 4×5 min frames 50–70 min after ^{18}F-florbetapir injection or 90–110 min after ^{18}F-florbetaben injection.[25] Tau-PET was acquired 75–105 min after injection of ^{18}F-flortaucipir in 6×5 min frames. All time frames were motion-corrected and averaged to obtain mean images (for details see http://adni.loni.usc.edu/methods/pet-analysis-method/pet-analysis/). Structural T_1-weighted MRI images were processed using the ANTs cortical thickness pipeline and parcellated with the Desikan–Killiany Atlas[51] and non-linearly registered to MNI space.[52] Amyloid-PET and tau-PET images were co-registered via native-space T_1-weighted images to MNI standard space using ANTs-derived normalization parameters. Global amyloid-PET SUVRs were intensity-normalized to the whole cerebellum and transformed to centiloid.[53] Partial volume-corrected global tau-PET SUVRs were obtained from the ADNI database, which were calculated using the inferior cerebellum as reference region and averaged across neocortical Desikan–Killiany atlas regions of interest (see here for details: https://ida.loni.usc.edu/login.jsp). Partial volume correction was performed by ADNI PET Core at UC Berkeley, using the geometric transfer method. For regional tau-PET SUVRs, we employed a congruent approach, applying geometric transfer method-based partial volume correction for cortical projections of white matter fibre tracts (PETPVC toolbox:[54] https://github.com/UCL/PETPVC). Specifically, we used the geometric transfer matrix approach to correct the region of interest-based tau-PET data for grey matter density using the segmented T_1-weighted image that was obtained in closest proximity to the tau-PET scan.

Statistical analyses

All statistical analyses were performed in R (version 3.6.1).[55] The statistical significance level was set at $\alpha < 0.05$.

To compare between controls and patients with respect to demographic characteristics, vascular risk factors, conventional MRI and PET markers, we used chi-squared (χ^2) tests (for categorical variables) and non-parametric Wilcoxon rank sum tests and Kruskal–Wallis tests (for continuous variables), as appropriate.

Next, we were interested in group differences in tract-specific fixel metrics between SVD and matched controls, and between groups with different biomarker status for Alzheimer's disease (Aβ+T– versus Aβ–T–, Aβ+T+ versus Aβ–T– and Aβ+T+ versus Aβ+T–). Because fixel metrics have been shown to be significantly influenced by head size,[56] we first regressed out the effect of intracranial volume and conducted subsequent analysis on residuals, i.e. fixel metrics corrected for head size ('stats' package). We then calculated the effect size for group comparisons in all predefined fibre tracts using Cohen's *d* ('psych' package).

Next, we performed simple linear regression analyses to explore associations between SVD and Alzheimer's disease typical imaging hallmarks (independent variable) and fibre density and fibre-bundle cross-section of the respective fibre tract (dependent variable, 'stats' package). For SVD hallmarks, we included WMHV, lacune and cerebral microbleed count. For Alzheimer's disease hallmarks, we included global amyloid-PET (centiloid), global tau-PET, regional tau-PET (i.e. tau-PET SUVR in cortical projections of the respective fibre tract). We also included normalized global brain volume indicative of neurodegeneration as an independent variable, which is associated with both Alzheimer's disease[3] and SVD.[57] Additionally, we assessed associations with age to ensure that potential associations were not driven by aging alone. In these regression analyses, we used the full extent of the SVD and Alzheimer's disease sample by also including the controls (but report subsequent sensitivity analyses in the CADASIL only and the Aβ+ only group in the Supplementary material). Effect sizes were determined by the adjusted R^2. *P*-values were adjusted with the false discovery rate per sample and fixel metric resulting in a maximum of 5% of false positives.

To assess the relative variable importance of disease markers in explaining fixel metrics, we performed multivariable random forest regression analyses with conditional inference trees in the Alzheimer's disease sample (R package 'party'). This machine-learning method overcomes the problem of multicollinearity within the disease markers. We focused on four variables of interest: WMHV as a marker for SVD, amyloid- and global tau-PET as a marker for Alzheimer's disease and brain volume as a marker for neurodegeneration. We repeated random forest regression 100 times to determine the point estimate and a 95% CI.

All analyses were conducted independently in each of the three samples.

Data availability

Anonymized data of the SVD and validation samples will be made available upon reasonable request to the corresponding author and only after permission of the regulatory bodies. ADNI data are freely available and can be retrieved from adni.loni.usc.edu upon registration to the ADNI database.

Results

Sample characteristics and demographics are shown in Table 1. As expected, SVD patients had higher WMHVs, more lacunes and microbleeds compared to controls ($P < 0.001$). SVD patients further had higher rates of hypercholesterolaemia than age-matched controls ($P < 0.05$). WMHV increased with progressing amyloid and tau pathology in the Alzheimer's disease sample ($P < 0.001$).

Fixel metric group comparisons

Genetically defined SVD predominantly leads to reduced fibre density

The fibre density of all white matter fibre tracts was reduced in SVD compared to controls [range of Cohen's *d* (0.33; 0.57), Fig. 4A and B and Supplementary Table 2]. Results for the fibre-bundle cross-section were less consistent. While the fibre-bundle cross-section of most fibre tracts was reduced in SVD compared to controls [Cohen's *d* (0.19; 0.35)], 11 tracts showed no group difference

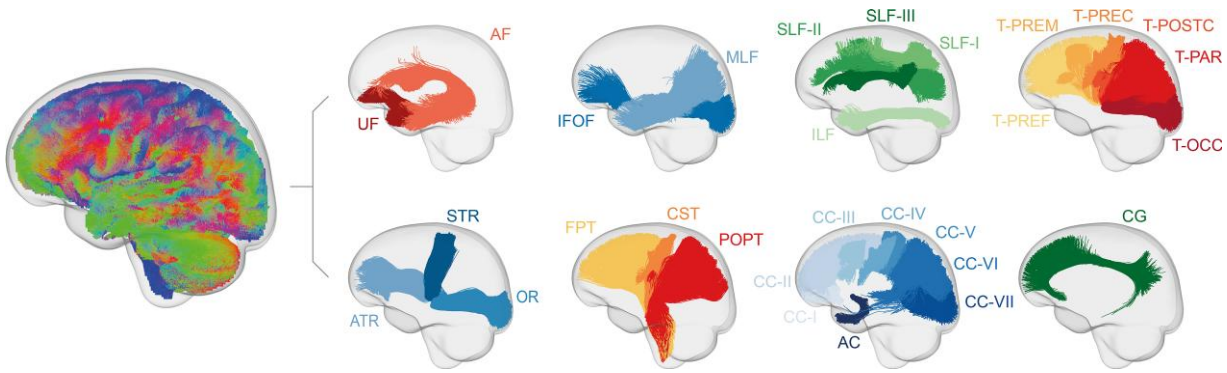

Figure 3 Sagittal view of investigated white matter fibre tracts. Tracts generated in fibre orientation distribution template space are shown for illustration. We analysed 29 white matter fibre tracts (only the left hemisphere is shown): AC = anterior commissure; AF = arcuate fasciculus; ATR = anterior thalamic radiation; CC-I to CC-VII = corpus callosum I to VII [CC-I: rostrum, CC-II: genu, CC-III: rostral body (premotor), CC-IV: anterior midbody (primary motor), CC-V: posterior midbody (primary somatosensory), CC-VI = isthmus, CC-VII: splenium]; CG = cingulum; CST = cortico-spinal tract; FPT = fronto-pontine tract; IFOF = inferior fronto-occipital fasciculus; ILF = inferior longitudinal fasciculus; MLF = middle longitudinal fasciculus; OR = optic radiation; POPT = parieto-occipital pontine; SLF-I to SLF-III = superior longitudinal fasciculus I to III; STR = superior thalamic radiation; T-OCC = thalamo-occipital; T-PAR = thalamo-parietal; T-POSTC = thalamo-postcentral; T-PREC = thalamo-precentral; T-PREF = thalamo-prefrontal; T-PREM = thalamo-premotor; UF = uncinate fasciculus.

Table 1 Sample characteristics

	SVD			Alzheimer's disease				Validation
	Control ($n = 22$)	CADASIL ($n = 73$)	P-value	Aβ−T− ($n = 34$)	Aβ+T− ($n = 19$)	Aβ+T+ ($n = 18$)	P-value	($n = 221$)
Demographic characteristics								
Age, years, median (IQR)	60 (21.5)	55 (14)	0.2084	72.50 (9.5)	78.70 (7.8)	75.05 (6.85)	0.1359	73.64 (9.67)
Female, *n* (%)	9 (41)	44 (60)	0.1744	19 (56)	10 (53)	8 (44)	0.7335	98 (44)
Vascular risk factors, *n* (%)								
Hypertension	5 (23)	17 (23)	1.0	10 (29)	9 (47)	10 (56)	0.1506	146 (66)
Hypercholesterolaemia	5 (23)	37 (51)	0.0471	9 (26)	3 (16)	8 (44)	0.1463	116 (52)
Diabetes	0 (0)	1 (0.01)	1.0	3 (9)	2 (11)	4 (22)	0.3647	33 (15)
Current or past smoking	9 (41)	44 (60)	0.2425	2 (6)	3 (16)	2 (11)	0.4994	143 (65)
PET markers, median (IQR)								
Amyloid-PET centiloid	-	-	-	−7.25 (11.91)	51.53 (38.26)	87.53 (46.41)	<0.0001	-
Global tau-PET SUVR	-	-	-	1.03 (0.12)	1.08 (0.10)	1.18 (0.30)	<0.0001	-
MRI markers, median (IQR)								
WMH volume,[a] %	0.03 (0.08)	4.58 (5.23)	<0.0001	0.24 (0.33)	0.53 (0.73)	0.69 (0.74)	0.0043	0.30 (0.69)
Lacune count	0 (0)	2 (7)	<0.0001	0 (0)	0 (0)	0 (0)	0.8763	0 (0)
Microbleed count	0 (0)	2 (7)	<0.0001	0 (0)	0 (0)	0 (0)	0.0160	0 (1)
Brain volume,[a] %	75.72 (7.64)	76.22 (8.46)	0.2024	70.79 (1.27)	70.00 (2.55)	70.31 (3.26)	0.4158	74.34 (5.65)

IQR = interquartile range; *n* = number.
[a]Normalized to the intracranial volume.

and the fibre-bundle cross-section of the anterior thalamic radiation and the first segment of the corpus callosum (rostrum) was even higher in SVD compared to controls (Cohen's $d = -0.33$, both tracts).

Both fibre density and fibre-bundle cross-section are reduced across the Alzheimer's disease spectrum

In the Alzheimer's disease sample, the Aβ+T− group showed consistently lower fibre density in most fibre tracts compared to the Aβ−T− control group [Cohen's d (0.27; 0.49), Fig. 4C and D and Supplementary Table 3]. The fibre-bundle cross-section was also reduced in the Aβ+T− group [Cohen's d (0.27; 0.51)]. Similarly, the Aβ+T+ group showed lower fibre density [Cohen's d (0.30; 0.43)] and lower fibre-bundle cross-section [Cohen's d (0.27; 0.40)] compared to the Aβ−T− control group.

To determine the extent to which these effects were driven by differences in SVD burden between groups, we included WMHV as covariate in a sensitivity analysis. This reduced effect sizes on average by 42% for fibre density and 8% for fibre-bundle cross-section (Aβ+T− versus Aβ−T−), and by 21% for fibre density and 7% for fibre-bundle cross-section (Aβ+T+ versus Aβ−T−; Supplementary Table 3).

The Aβ+T+ group did not show any additional white matter damage regarding fibre density or fibre-bundle cross-section compared to Aβ+T−. In summary, both fibre density and fibre-bundle cross-section were reduced in the presence of amyloid pathology, but not further altered by additional tau pathology.

Associations with disease markers

Reduced fibre density is mainly associated with higher SVD burden

In simple linear regression in the SVD sample, fibre density of all fibre tracts was strongly associated with WMHV [range of R^2_{adj} (0.29; 0.79)], lacunes [R^2_{adj} (0.12; 0.48)] and microbleeds [R^2_{adj} (0.16; 0.43), Fig. 5A and Supplementary Table 4]. In contrast, effect sizes were

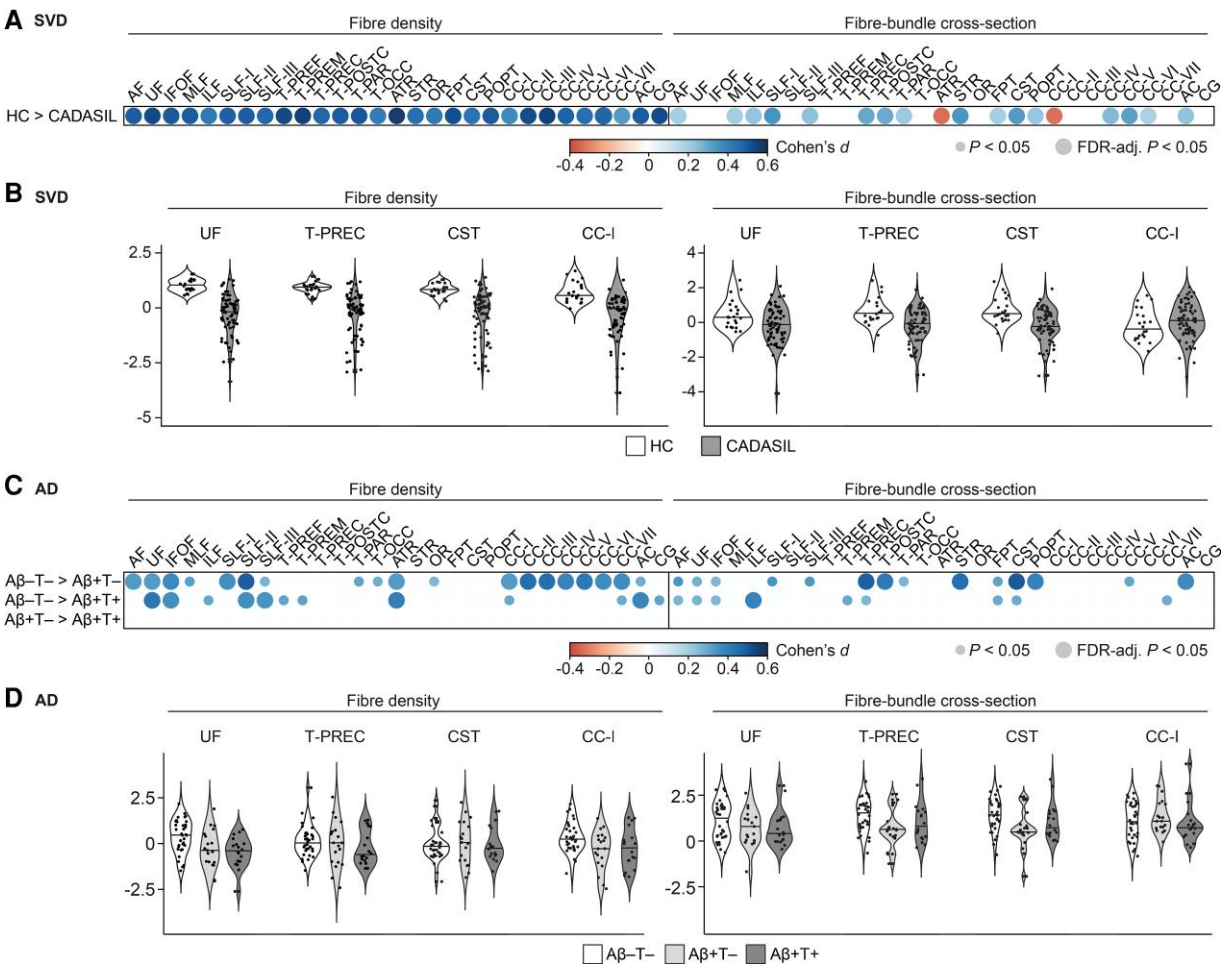

Figure 4 Group comparisons of fixel metrics. (**A**) Difference in fixel metrics between age-matched healthy controls (HC) and CADASIL patients in the SVD sample quantified with Cohen's *d* represented by colour. Circle size depicts statistical significance level. (**B**) Violin plots of fixel metrics of four representative fibre tracts in the SVD sample for exemplary illustration. (**C**) Difference in fixel metrics between age-matched Aβ–T– and Aβ+T–; Aβ–T– and Aβ+T+; Aβ+T– and Aβ+T+ quantified with Cohen's *d* represented by colour. Circle size depicts statistical significance level. (**D**) Violin plots of fixel metrics of the same four tracts in the Alzheimer's disease sample. Refer to Fig. 3 for abbreviations of the fibre tracts.

small for associations with age [R^2_{adj} (0.03; 0.13)] and brain volume [R^2_{adj} (0.05; 0.16)].

Fibre-bundle cross-section was also associated with WMHV, but with smaller effect sizes [R^2_{adj} (0.06; 0.43)], as well as with lacune count [R^2_{adj} (0.06; 0.52)], microbleed count [R^2_{adj} (0.07; 0.38)] and brain volume [R^2_{adj} (0.05; 0.29)]. Effect sizes were small for associations with age [age: R^2_{adj} (0.04; 0.13)].

Findings could be replicated when assessing associations in CADASIL patients only (Supplementary Fig. 1A).

Reduced fibre-bundle cross-section is mainly associated with cerebral atrophy in the Alzheimer's disease sample

In simple linear regression analyses, fibre density in the Alzheimer's disease sample was likewise associated with WMHV [R^2_{adj} (0.04; 0.20), Fig. 5B and Supplementary Table 5] and to some extent with microbleed count [R^2_{adj} (0.05; 0.08)] but not with lacune count, which was expected given the low number of lacunes and microbleeds in this sample (Table 1). Fibre density was not associated with brain volume and with age only in selected fibre tracts [R^2_{adj} (0.05; 0.17)]. Effect sizes for associations with Alzheimer's disease PET markers were substantially smaller than with SVD MRI markers [amyloid-PET: R^2_{adj} (0.04; 0.11) and tau-PET: R^2_{adj} (0.04)].

Compared to fibre density, fibre-bundle cross-section was less associated with SVD imaging markers [WMHV: R^2_{adj} (0.04; 0.06); no significant associations with lacunes or microbleeds]. In contrast, fibre-bundle cross-section of all fibre tracts was strongly associated with brain volume [R^2_{adj} (0.06; 0.35)] and to some extent with age [R^2_{adj} (0.04; 0.20)]. Associations with Alzheimer's disease PET markers were mostly absent or showed only small effect sizes [amyloid-PET: R^2_{adj} (0.04; 0.05); tau-PET: R^2_{adj} (0.05; 0.06)].

All findings could be replicated when assessing associations in Aβ+ study participants only, except for associations with Alzheimer's disease PET markers, which were even weaker (Supplementary Fig. 1B).

In multivariable random forest regression analyses (Fig. 6), WMHV showed the highest variable importance for fibre density in most fibre tracts, while brain volume showed the highest variable importance for fibre bundle cross-section in all tracts.

Fibre density is associated with SVD markers and fibre-bundle cross-section with brain volume in presumed mixed pathology

Also in the validation sample, fibre density of all tracts was highly associated with WMHV [R^2_{adj} (0.08; 0.48), Fig. 5C and

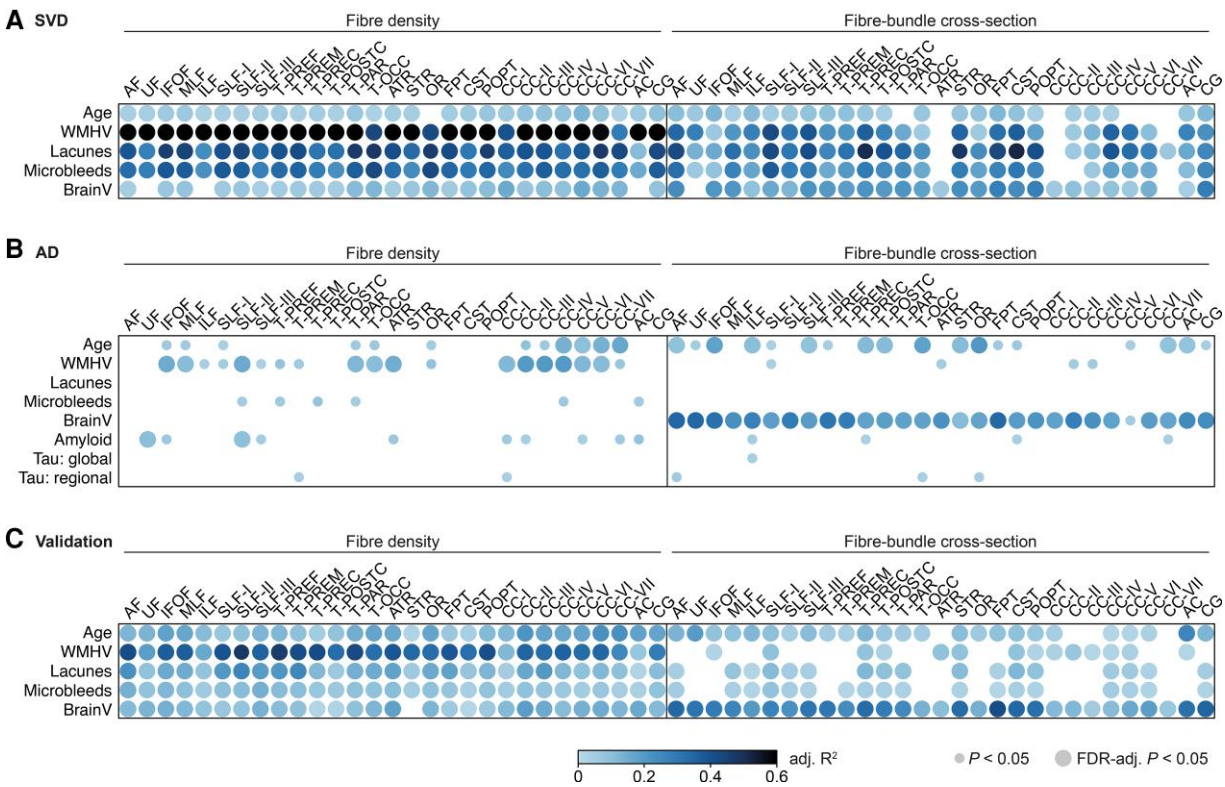

Figure 5 Associations with disease markers. Effect sizes (adj. R^2) obtained from simple linear regression analyses are represented by colour. Circle size depicts statistical significance level. Associations between fixel metrics of white matter fibre tracts and disease markers were assessed in (**A**) the SVD sample, (**B**) the Alzheimer's disease sample—including in addition amyloid-PET and tau-PET markers—and (**C**) the validation sample. Refer to Fig. 3 for abbreviations of the fibre tracts. BrainV = brain volume.

Supplementary Table 6]. Fibre density of all tracts was also (with smaller effect sizes) associated with lacune count [R^2_{adj} (0.03; 0.26)], microbleed count [R^2_{adj} (0.04; 0.15)], brain volume (R^2_{adj} (0.01; 0.19)] and age [R^2_{adj} (0.03; 0.23)].

Effect sizes were small for associations between fibre-bundle cross-section and WMHV [R^2_{adj} (0.02; 0.09)]; lacune count [R^2_{adj} (0.02; 0.13)] and microbleed count [R^2_{adj} (0.02; 0.09)]. Effect sizes were largest for brain volume [R^2_{adj} (0.06; 0.42)].

Results of group comparisons and associations with disease markers of the combined metric fibre density and bundle cross-section can be found in the Supplementary material as well as scatterplots of the most important findings (Supplementary Figs 2–5).

Discussion

Our multimodal neuroimaging study systematically assessed the utility of fixel-based, tract-specific diffusion metrics to disentangle the effects of Alzheimer's disease and SVD on white matter. Our main findings are that (i) fibre density was markedly reduced in genetically defined SVD and showed the strongest association with SVD imaging hallmarks; (ii) fibre-bundle cross-section was mainly associated with brain volume, especially in the Alzheimer's disease sample; and (iii) both fibre density and fibre-bundle cross-section were reduced in the presence of amyloid, but this was not further exacerbated by abnormal tau deposition. Taken together, our results suggest that the white matter microstructure metric fibre density is primarily determined by SVD, while the macrostructure metric fibre-bundle cross-section is strongly associated with neurodegeneration. Importantly, the ability of fixel metrics to capture distinct effects of SVD and neurodegeneration was validated in an independent sample.

The marked reduction of the microscopic feature fibre density with increasing SVD burden might result from increased extracellular water moving axons further apart.[21] In line with this, we previously demonstrated that diffusion tensor imaging alterations in SVD are mainly determined by increases in extracellular free water.[58] In addition, a reduction in apparent fibre density (although not assessed using fixel-based analysis) has been suggested to accompany an increase in extracellular water within WMH of CADASIL patients.[59] Vascular oedema, e.g. resulting from blood–brainbarrier leakage in SVD, might be a main driver of this fluid shift.[5,60] Interestingly, while the fibre density decreased, we observed in the genetically defined SVD sample a simultaneous increase in the fibre-bundle cross-section of two tracts, the anterior thalamic radiation and the first segment of the corpus callosum (rostrum, harbouring parts of the forceps minor). Strikingly, the anterior thalamic radiation and forceps minor were previously identified as strategic locations for processing speed performance in SVD,[61,62] the core cognitive deficit of the disease. One might speculate that the expansion of the extracellular space following vascular oedema led to a swelling of these fibre tracts which is captured by an increase in fibre-bundle cross-section.[21,60]

The macroscopic feature fibre-bundle cross-section was most prominently reduced with increasing amyloid pathology in group comparisons and strongly associated with cerebral atrophy as a proxy of neurodegeneration in the Alzheimer's disease and validation sample. Together with the finding that brain volume was

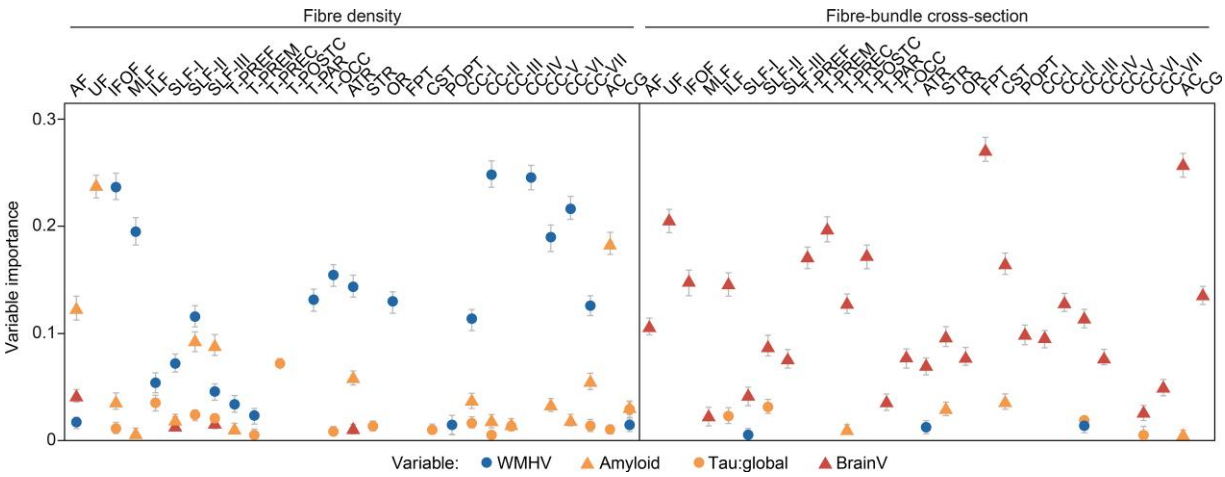

Figure 6 Multivariable analyses. Random forest regression analyses for estimating the relative variable importance for the SVD marker WMHV (blue), markers of primary Alzheimer's disease pathology (orange) and brain volume (BrainV, red) with regard to tract-specific fixel metrics in the Alzheimer's disease sample. Plots indicate point estimate and 95% CI for the conditional variable importance. Refer to Fig. 3 for abbreviations of the fibre tracts.

not or only weakly associated with fibre density, this suggests that in fixel-based analysis, neurodegeneration predominantly manifests in alterations of white matter macrostructure, but not microstructure. Thus, fibre-bundle cross-section indeed seems to be reflective of the accumulated axon loss as previously postulated.[19]

While associations in the SVD sample were strongest for fibre density, and in the Alzheimer's disease sample for fibre-bundle cross-section, both associations were found in the validation sample with mixed pathologies, supporting the concept that both SVD and Alzheimer's disease contribute to white matter damage in mixed disease.

In the Alzheimer's disease sample, both fibre density and fibre-bundle cross-section were reduced upon amyloid pathology in group comparisons, which might seem counterintuitive at first. As expected from epidemiological and histopathology studies,[6,7] concomitant SVD was found in the Alzheimer's disease sample, with the largest difference in WMH burden between the A+T– group and matched A–T– controls. Controlling for this group difference in WMH volume attenuated the observed effects of amyloid, especially on fibre density. Thus, the effect of amyloid on fibre density can at least partly be explained by concomitant SVD, which is plausible given the likely presence of cerebral amyloid angiopathy, which is also captured by amyloid-PET.[63,64]

Brain atrophy clearly showed the strongest associations with fixel metrics, i.e. fibre-bundle cross-section, in the Alzheimer's disease sample. However, in contrast to a previously postulated hypothesis,[65] we did not find that cortical tau pathology is a main driver of alterations in fixel metrics.

While many studies investigated white matter alterations in SVD or Alzheimer's disease using models operating on the voxel level,[9] such as diffusion tensor imaging and more advanced diffusion models,[66] only very few studies have so far utilized fixel-based analysis. Importantly, none of the prior fixel-based studies considered mixed disease, but studied either SVD or Alzheimer's disease in isolation, thus ignoring the crucial aspect of concomitant pathologies. Despite technical limitations,[21,67] it was recently shown that fibre density obtained from fixel-based analysis is highly sensitive towards processing speed deficits in sporadic SVD,[68] confirming previous findings from voxel-based analysis. The aforementioned fixel-based analysis study in Alzheimer's disease reported a reduction in both fibre density and fibre-bundle cross-section in MCI and Alzheimer's disease patients.[22] However, besides not considering concomitant SVD, a full Alzheimer's disease biomarker characterization was not possible due to prematurity of tau-PET tracers upon data collection of that study.[69] By considering both pathologies and by including data from both amyloid- and tau-PET, we were able to substantially extend previous results, close crucial knowledge gaps and derive insights highly relevant for both future research studies and potentially also clinical applications.

Our study has some potential limitations. First, in the mixed pathology sample Alzheimer's disease biomarkers were not available, precluding an independent validation of results for the direct effects of amyloid and tau pathology. Second, while all samples had diffusion MRI data suitable for fixel-based analysis, the acquisition was not harmonized across the three samples. However, this can also be regarded as a strength in terms of generalizability and independent validation of findings, because despite differences in the MRI acquisition, we found consistent results across all three samples. MRI data in the Alzheimer's disease sample were acquired across 13 different scanners. Scanner effects were mitigated by selecting only acquisitions with identical parameters and an intensity normalization step. Eventually, excellent intersite reproducibility of fixel metrics (Supplementary material) enabled pooling of data from different scanners. Lastly, amyloid-PET data were not partial volume-corrected due to centiloid transformation,[70] hence our results warrant further replication using a large single tracer data set.

A main strength of this study is the extensive biomarker characterization, including multiple markers for SVD as well as amyloid- and tau-PET data in the Alzheimer's disease sample. This enabled a multimodal approach, which was deemed essential in further validation of fixel-based metrics by the developers of the method.[21] Unlike in the Alzheimer's disease field, truly SVD-specific biomarkers are still lacking. To overcome this limitation, we included the sample of genetically defined SVD patients. Because these patients were relatively young, concomitant Alzheimer's disease and other age-related neurodegenerative pathology can be regarded as rare, thus enabling the unique opportunity to study pure SVD without the need for biomarker characterization. While data from autosomal dominant Alzheimer's disease would have perfectly

complemented our analysis in this regard, we are not aware of any familial Alzheimer's disease studies with diffusion MRI data suitable for fixel-based analysis.

The ability of the fixel-based analysis to identify distinct effects of SVD and neurodegeneration on white matter opens a path towards personalized medicine. Future work should address the ability of fixel-derived diffusion markers to explain the extent to which SVD and neurodegeneration contribute to cognitive impairment in mixed disease. This would enable disease-specific interventions targeting Alzheimer's disease- or SVD-related brain alterations rather than managing disease-shared risk factors. Our results illustrate once more that it is mandatory to consider SVD when assessing white matter integrity in the context of dementia studies and trials. Furthermore, longitudinal studies are required to capture temporal dynamics of fibre density and fibre-bundle cross-section. Given recent indications for SVD lesion regression,[71] it remains to be assessed whether the reduction in fibre density observed in SVD is irreversible and how it changes upon disease intervention, e.g. intensified risk factor treatment. Technical validation studies, assessing test–retest reliability and intersite reproducibility of these novel markers in patients, will be essential for developing a surrogate endpoint for clinical trials.

In conclusion, our results show that fibre density and fibre-bundle cross-section, obtained from fixel-based analysis of diffusion MRI data, allow identification of distinct effects of SVD and neurodegeneration on white matter integrity. While white matter microstructure is predominantly determined by SVD, neurodegeneration leads to alterations in white matter macrostructure. Leveraging these distinct effects, fixel-based white matter analysis can propel future research, clinical trials targeting disease-specific mechanisms and clinical applications in the context of precision medicine.

Acknowledgements

Data used in preparation of this article were obtained from the Munich cohort of the ZOOM@SVDs study, which is part of the SVDs@target project. As such, the investigators within the ZOOM@SVDs study contributed to the design but did not participate in analysis or writing of this report. Data used in preparation of this article were obtained from the Alzheimer's Disease Neuroimaging Initiative (ADNI) database (adni.loni.usc.edu). As such, the investigators within the ADNI contributed to the design and implementation of ADNI and/or provided data but did not participate in analysis or writing of this report. A complete listing of ADNI investigators can be found at: http://adni.loni.usc.edu/wp-content/uploads/how_to_apply/ADNI_Acknowledgement_List.pdf

Funding

This project has received funding from the European Union's Horizon 2020 research and innovation programme No. 666881, SVDs@target (to M. Dichgans), the DFG as part of the Munich Cluster for Systems Neurology (EXC 2145 SyNergy—ID 390857198) and the Stiftung zur Erforschung der Vaskulären Demenz. M.C. was supported by China Scholarship Council (201706100189). A.M.T. is a junior staff member of the Dutch Heart Foundation (grant number 2016T044). Data collection and sharing for this project was funded by the Alzheimer's Disease Neuroimaging Initiative (ADNI) (National Institutes of Health Grant U01 AG024904) and DOD ADNI (Department of Defense award number W81XWH-12-2-0012). ADNI is funded by the National Institute on Aging, the National Institute of Biomedical Imaging and Bioengineering and through generous contributions from the following: AbbVie; Alzheimer's Association; Alzheimer's Drug Discovery Foundation; Araclon Biotech; BioClinica, Inc.; Biogen; Bristol-Myers Squibb Company; CereSpir, Inc.; Cogstate; Esai Incorporated.; Elan Pharma International.; Eli Lilly and Company; EuroImmun; F. Hoffmann-La Roche Ltd and its affiliated company Genentech, Inc.; Fujirebio; GE Healthcare; IXICO.; Janssen Alzheimer Immunotherapy Research and Development; Johnson and Johnson Pharmaceutical Research and Development; Lumosity; Lundbeck; Merck & Co., Inc.; Meso Scale Diagnostics, LLC; NeuroRx Research; Neurotrack Technologies; Novartis Pharmaceuticals Corporation; Pfizer Inc.; Piramal Imaging; Servier; Takeda Pharmaceutical Company; and Transition Therapeutics. The Canadian Institutes of Health Research is providing funds to support ADNI clinical sites in Canada. Private-sector contributions are facilitated by the Foundation for the National Institutes of Health (www.fnih.org). The grantee organization is the Northern California Institute for Research and Education and the study is coordinated by the Alzheimer's Therapeutic Research Institute at the University of Southern California. ADNI data are disseminated by the Laboratory for Neuro Imaging at the University of Southern California.

Competing interests

The authors report no competing interests.

Supplementary material

Supplementary material is available at *Brain* online.

References

1. van der Flier WM, Skoog I, Schneider JA, *et al*. Vascular cognitive impairment. *Nat Rev Dis Primer*. 2018;4(1):1–16.
2. Dichgans M, Leys D. Vascular cognitive impairment. *Circ Res*. 2017;120(3):573–591.
3. Jack CR, Bennett DA, Blennow K, *et al*. NIA-AA Research framework: Toward a biological definition of Alzheimer's disease. *Alzheimers Dement*. 2018;14(4):535–562.
4. Wardlaw JM, Smith EE, Biessels GJ, *et al*. Neuroimaging standards for research into small vessel disease and its contribution to ageing and neurodegeneration. *Lancet Neurol*. 2013;12(8):822–838.
5. Wardlaw JM, Smith C, Dichgans M. Small vessel disease: mechanisms and clinical implications. *Lancet Neurol*. 2019;18(7):684–696.
6. Kapasi A, DeCarli C, Schneider JA. Impact of multiple pathologies on the threshold for clinically overt dementia. *Acta Neuropathol (Berl)*. 2017;134(2):171–186.
7. Attems J, Jellinger KA. The overlap between vascular disease and Alzheimer's disease—Lessons from pathology. *BMC Med*. 2014;12(1):1–12.
8. Beach TG, Malek-Ahmadi M. Alzheimer's disease neuropathological comorbidities are common in the younger-old. *J Alzheimers Dis*. 2021;79(1):389–400.
9. Raja R, Rosenberg G, Caprihan A. Review of diffusion MRI studies in chronic white matter diseases. *Neurosci Lett*. 2019;694:198–207.
10. Baykara E, Gesierich B, Adam R, *et al*. A novel imaging marker for small vessel disease based on skeletonization of white matter tracts and diffusion histograms. *Ann Neurol*. 2016;80(4):581–592.

11. Pichet Binette A, Theaud G, Rheault F, *et al*. Bundle-specific associations between white matter microstructure and Aβ and tau pathology in preclinical Alzheimer's disease. *eLife*. 2021;10:e62929.
12. Nasrabady SE, Rizvi B, Goldman JE, Brickman AM. White matter changes in Alzheimer's disease: A focus on myelin and oligodendrocytes. *Acta Neuropathol Commun*. 2018;6(1):22.
13. Finsterwalder S, Vlegels N, Gesierich B, *et al*. Small vessel disease more than Alzheimer's disease determines diffusion MRI alterations in memory clinic patients. *Alzheimers Dement*. 2020; 16(11):1504–1514.
14. Vemuri P, Lesnick TG, Knopman DS, *et al*. Amyloid, vascular, and resilience pathways associated with cognitive aging. *Ann Neurol*. 2019;86(6):866–877.
15. Raghavan S, Przybelski SA, Reid RI, *et al*. White matter damage due to vascular, tau, and TDP-43 pathologies and its relevance to cognition. *Acta Neuropathol Commun*. 2022;10(1):16.
16. Jones DK, Knösche TR, Turner R. White matter integrity, fiber count, and other fallacies: The do's and don'ts of diffusion MRI. *NeuroImage*. 2013;73:239–254.
17. Tournier JD, Calamante F, Connelly A. MRtrix: Diffusion tractography in crossing fiber regions. *Int J Imaging Syst Technol*. 2012; 22(1):53–66.
18. Jeurissen B, Leemans A, Tournier JD, Jones DK, Sijbers J. Investigating the prevalence of complex fiber configurations in white matter tissue with diffusion magnetic resonance imaging. *Hum Brain Mapp*. 2013;34(11):2747–2766.
19. Raffelt DA, Tournier JD, Smith RE, *et al*. Investigating white matter fibre density and morphology using fixel-based analysis. *NeuroImage*. 2017;144:58–73.
20. Raffelt D, Tournier JD, Rose S, *et al*. Apparent fibre density: A novel measure for the analysis of diffusion-weighted magnetic resonance images. *NeuroImage*. 2012;59(4):3976–3994.
21. Dhollander T, Clemente A, Singh M, *et al*. Fixel-based analysis of diffusion MRI: Methods, applications, challenges and opportunities. *NeuroImage*. 2021;241:118417.
22. Mito R, Raffelt D, Dhollander T, *et al*. Fibre-specific white matter reductions in Alzheimer's disease and mild cognitive impairment. *Brain*. 2018;141(3):888–902.
23. van den Brink H, Kopczak A, Arts T, *et al*. Zooming in on cerebral small vessel function in small vessel diseases with 7 T MRI: Rationale and design of the "ZOOM@SVDs" study. *Cereb Circ Cogn Behav*. 2021;2:100013.
24. Weiner MW, Veitch DP, Aisen PS, *et al*. The Alzheimer's Disease Neuroimaging Initiative 3: Continued innovation for clinical trial improvement. *Alzheimers Dement*. 2017;13(5):561–571.
25. Landau SM, Mintun MA, Joshi AD, *et al*. Amyloid deposition, hypometabolism, and longitudinal cognitive decline. *Ann Neurol*. 2012;72(4):578–586.
26. Biel D, Brendel M, Rubinski A, *et al*. Tau-PET and *in vivo* Braak-staging as prognostic markers of future cognitive decline in cognitively normal to demented individuals. *Alzheimers Res Ther*. 2021;13(1):137.
27. Schöll M, Lockhart SN, Schonhaut DR, *et al*. PET imaging of tau deposition in the aging human brain. *Neuron*. 2016;89(5):971–982.
28. van Norden AG, de Laat KF, Gons RA, *et al*. Causes and consequences of cerebral small vessel disease. The RUN DMC study: A prospective cohort study. Study rationale and protocol. *BMC Neurol*. 2011;11(1):29.
29. Tuladhar AM, van Uden IWM, Rutten-Jacobs LCA, *et al*. Structural network efficiency predicts conversion to dementia. *Neurology*. 2016;86(12):1112–1119.
30. Andersson JLR, Skare S, Ashburner J. How to correct susceptibility distortions in spin-echo echo-planar images: Application to diffusion tensor imaging. *NeuroImage*. 2003;20(2):870–888.
31. Smith SM, Jenkinson M, Woolrich MW, *et al*. Advances in functional and structural MR image analysis and implementation as FSL. *NeuroImage*. 2004;23:S208–S219.
32. Andermatt S, Pezold S, Cattin PC. Automated segmentation of multiple sclerosis lesions using multi-dimensional gated recurrent units. In: Crimi A, Bakas S, Kuijf H, Menze B, Reyes M, eds. *Brainlesion: Glioma, multiple sclerosis, stroke and traumatic brain injuries*. Lecture Notes in Computer Science. Springer International Publishing; 2018:31–42.
33. Puonti O, Iglesias JE, Van Leemput K. Fast and sequence-adaptive whole-brain segmentation using parametric Bayesian modeling. *NeuroImage*. 2016;143:235–249.
34. ter Telgte A, Wiegertjes K, Tuladhar AM, *et al*. Investigating the origin and evolution of cerebral small vessel disease: The RUN DMC–InTENse study. *Eur Stroke J*. 2018;3(4):369–378.
35. Dewenter A, Gesierich B, ter Telgte A, *et al*. Systematic validation of structural brain networks in cerebral small vessel disease. *J Cereb Blood Flow Metab*. 2022;42:1020–1032.
36. Veraart J, Novikov DS, Christiaens D, Ades-aron B, Sijbers J, Fieremans E. Denoising of diffusion MRI using random matrix theory. *NeuroImage*. 2016;142:394–406.
37. Veraart J, Fieremans E, Novikov DS. Diffusion MRI noise mapping using random matrix theory. *Magn Reson Med*. 2016;76(5): 1582–1593.
38. Cordero-Grande L, Christiaens D, Hutter J, Price AN, Hajnal JV. Complex diffusion-weighted image estimation via matrix recovery under general noise models. *NeuroImage*. 2019;200: 391–404.
39. Tournier JD, Smith R, Raffelt D, *et al*. MRtrix3: A fast, flexible and open software framework for medical image processing and visualisation. *NeuroImage*. 2019;202:116137.
40. Kellner E, Dhital B, Kiselev VG, Reisert M. Gibbs-ringing artifact removal based on local subvoxel-shifts. *Magn Reson Med*. 2016; 76(5):1574–1581.
41. Andersson JLR, Sotiropoulos SN. An integrated approach to correction for off-resonance effects and subject movement in diffusion MR imaging. *NeuroImage*. 2016;125:1063–1078.
42. Andersson JLR, Graham MS, Zsoldos E, Sotiropoulos SN. Incorporating outlier detection and replacement into a non-parametric framework for movement and distortion correction of diffusion MR images. *NeuroImage*. 2016;141:556–572.
43. Andersson JLR, Graham MS, Drobnjak I, Zhang H, Filippini N, Bastiani M. Towards a comprehensive framework for movement and distortion correction of diffusion MR images: Within volume movement. *NeuroImage*. 2017;152:450–466.
44. Andersson JLR, Graham MS, Drobnjak I, Zhang H, Campbell J. Susceptibility-induced distortion that varies due to motion: Correction in diffusion MR without acquiring additional data. *NeuroImage*. 2018;171:277–295.
45. Schilling KG, Blaber J, Hansen C, *et al*. Distortion correction of diffusion weighted MRI without reverse phase-encoding scans or field-maps. *PLOS ONE*. 2020;15(7):e0236418.
46. Schilling KG, Blaber J, Huo Y, *et al*. Synthesized b0 for diffusion distortion correction (Synb0-DisCo). *Magn Reson Imaging*. 2019; 64:62–70.
47. Jeurissen B, Tournier JD, Dhollander T, Connelly A, Sijbers J. Multi-tissue constrained spherical deconvolution for improved analysis of multi-shell diffusion MRI data. *NeuroImage*. 2014;103: 411–426.
48. Dhollander T, Mito R, Raffelt D, Connelly A . Improved white matter response function estimation for 3-tissue constrained spherical deconvolution. *Proceedings of the 27th annual meeting of the International Society of Magnetic Resonance in Medicine* 2019:555.

49. Wasserthal J, Neher P, Maier-Hein KH. TractSeg—Fast and accurate white matter tract segmentation. *NeuroImage*. 2018;183:239–253.
50. Avants BB, Tustison NJ, Song G, Cook PA, Klein A, Gee JC. A reproducible evaluation of ANTs similarity metric performance in brain image registration. *NeuroImage*. 2011;54(3):2033–2044.
51. Desikan RS, Ségonne F, Fischl B, *et al*. An automated labeling system for subdividing the human cerebral cortex on MRI scans into gyral based regions of interest. *NeuroImage*. 2006;31(3):968–980.
52. Tustison NJ, Cook PA, Klein A, *et al*. Large-scale evaluation of ANTs and FreeSurfer cortical thickness measurements. *NeuroImage*. 2014;99:166–179.
53. Klunk WE, Koeppe RA, Price JC, *et al*. The centiloid project: Standardizing quantitative amyloid plaque estimation by PET. *Alzheimers Dement J Alzheimers Assoc*. 2015;11(1):1–15.e4.
54. Thomas BA, Cuplov V, Bousse A, *et al*. PETPVC: A toolbox for performing partial volume correction techniques in positron emission tomography. *Phys Med Biol*. 2016;61(22):7975–7993.
55. R Core Team. R: A language and environment for statistical computing. *Vienna R Found Stat Comput*. Published online 2016.
56. Smith R, Dhollander T, Connelly A. On the regression of intracranial volume in Fixel-Based Analysis. *27th International Society of Magnetic Resonance in Medicine* 2019;27:3385.
57. Smith EE, Biessels GJ, De Guio F, *et al*. Harmonizing brain magnetic resonance imaging methods for vascular contributions to neurodegeneration. *Alzheimers Dement Diagn Assess Dis Monit*. 2019;11:191–204.
58. Duering M, Finsterwalder S, Baykara E, *et al*. Free water determines diffusion alterations and clinical status in cerebral small vessel disease. *Alzheimers Dement J Alzheimers Assoc*. 2018;14(6):764–774.
59. Yu X, Yin X, Hong H, *et al*. Increased extracellular fluid is associated with white matter fiber degeneration in CADASIL: *In vivo* evidence from diffusion magnetic resonance imaging. *Fluids Barriers CNS*. 2021;18:29.
60. De Guio F, Mangin JF, Duering M, Ropele S, Chabriat H, Jouvent E. White matter edema at the early stage of cerebral autosomal-dominant arteriopathy with subcortical infarcts and leukoencephalopathy. *Stroke*. 2015;46(1):258–261.
61. Duering M, Gesierich B, Seiler S, *et al*. Strategic white matter tracts for processing speed deficits in age-related small vessel disease. *Neurology*. 2014;82(22):1946–1950.
62. Duering M, Zieren N, Hervé D, *et al*. Strategic role of frontal white matter tracts in vascular cognitive impairment: A voxel-based lesion-symptom mapping study in CADASIL. *Brain J Neurol*. 2011;134(Pt 8):2366–2375.
63. Charidimou A, Farid K, Baron JC. Amyloid-PET in sporadic cerebral amyloid angiopathy: A diagnostic accuracy meta-analysis. *Neurology*. 2017;89(14):1490–1498.
64. Gurol ME, Becker JA, Fotiadis P, *et al*. Florbetapir-PET to diagnose cerebral amyloid angiopathy. *Neurology*. 2016;87(19):2043–2049.
65. McAleese KE, Walker L, Colloby SJ, *et al*. Cortical tau pathology: A major player in fibre-specific white matter reductions in Alzheimer's disease? *Brain*. 2018;141(6):e44-e44.
66. Konieczny MJ, Dewenter A, ter Telgte A, *et al*. Multi-shell diffusion MRI models for white matter characterization in cerebral small vessel disease. *Neurology*. 2021;96(5):e698–e708.
67. Genc S, Tax CMW, Raven EP, Chamberland M, Parker GD, Jones DK. Impact of b-value on estimates of apparent fibre density. *Hum Brain Mapp*. 2020;41(10):2583–2595.
68. Petersen M, Frey BM, Mayer C, *et al*. Fixel based analysis of white matter alterations in early stage cerebral small vessel disease. *Sci Rep*. 2022;12(1):1581.
69. Mito R, Raffelt D, Dhollander T, *et al*. Reply: Cortical tau pathology: A major player in fibre-specific white matter reductions in Alzheimer's disease? *Brain*. 2018;141(6):e45–e45.
70. La Joie R, Visani AV, Baker SL, *et al*. Prospective longitudinal atrophy in Alzheimer's disease correlates with the intensity and topography of baseline tau-PET. *Sci Transl Med*. 2020;12(524):eaau5732.
71. van Leijsen EMC, de Leeuw FE, Tuladhar AM. Disease progression and regression in sporadic small vessel disease-insights from neuroimaging. *Clin Sci Lond Engl 1979*. 2017;131(12):1191–1206.